McKelvey School of Engineering Theses & Dissertations

McKelvey School of Engineering

Spring 5-15-2017

Uncertainty Quantification of Wall-Modeled Large Eddy Simulation (WMLES) Model in OpenFOAM

Zuoxian Hou
Washington University in St. Louis

Follow this and additional works at: https://openscholarship.wustl.edu/eng_etds

Part of the Engineering Commons

Recommended Citation

WASHINGTON UNIVERSITY IN ST. LOUIS

School of Engineering and Applied Science
Department of Mechanical Engineering and Material Science

Thesis Examination Committee:
Ramesh Agarwal, Chair
Dave Peters
Swami Karunamoorthy

Uncertainty Quantification of Wall-Modeled Large Eddy Simulation (WMLES) Model in
OpenFOAM
by
Zuoxian Hou

A dissertation presented to the School of Engineering and Applied Science
of Washington University in St. Louis in partial fulfillment of the
requirements for the degree of
Master of Science

May 2017
St. Louis, Missouri

Table of Contents

List of Figures

List of Tables

<u>Acknowledgments</u>

I would like to thank to my parents, Yuhui Hou and Huan Wang, who taught me to be curious to everything and spirit of persistence in achieving the goal. I am grateful for their help in all aspects.

Many thanks to my research advisor, Professor Ramesh K Agarwal for providing me enormous help and guidance to improve my research skills. I would not have succeeded without his help. Thanks to Prof. Peters and Prof. Karunamoorthy for agreeing to serve on the thesis committee. I would like to thank Xu Han for providing enormous technical support in using the OpenFOAM and giving me confidence when I was disappointed. I would also like to thank Tim Wray and Issac Witte for teaching me how to use DAKOTA.

Finally, I want to thank to all my colleagues in the CFD lab. I had a meaningful and very pleasant time with all of them.

Zuoxian Hou

Washington University in St. Louis

May 2017

Dedicated to my parents.

ABSTRACT OF THESIS

Uncertainty Quantification of Wall-Modeled Large Eddy Simulation (WMLES) Model in

OpenFOAM

by

Zuoxian Hou

Master of Science in Mechanical Engineering

Washington University in St. Louis, 2017

Research Advisor: Professor Ramesh K. Agarwal

In this thesis, a non-intrusive uncertainty quantification (UQ) method is used to improve the accuracy of a wall-modeled large eddy simulation (WMLES) model. Detailed UQ studies focusing on the closure coefficients of two LES models are performed. A non-intrusive polynomial chaos model is used to evaluate output sensitivities and uncertainties in the entire flow domain. The proposed UQ method allows for the investigation of specific flow features and phenomena within the domain. The results of the UQ analyses are then used to identify which turbulence model closure coefficients most influence the flow features of interest. Sobol indices of closure coefficients (C_k, C_ε in Smagorinsky model and $C_k, C_\varepsilon, \kappa, A^+$ in WMLES model) are obtained. Based on the magnitudes of Sobol indices, refinements are then made to the closure coefficients of interest to improve the accuracy of the turbulence models. OpenFOAM is used as the flow solver and the UQ analyses are conducted with DAKOTA. The UQ method is applied to the channel flow at different Reynolds numbers. The refined LES turbulence models with modified closure coefficients show improvement in the prediction of the skin-friction coefficient in the channel flow.

Chapter 1: Introduction

1.1 Motivation

Interest in uncertainty quantification (UQ) in computational fluid dynamics (CFD) has grown in recent years. UQ has been successfully applied to design, optimization, and modeling problems, and is becoming a standard tool for verification and validation of numerical solutions. The development of non-intrusive UQ methods has reduced the computational expense of UQ and has allowed uncertainty propagation through complex models without alteration to the underlying model.

In the present work, the sensitivities of the closure coefficients of the LES Smagorinsky model, and the wall-modeled large eddy simulation (WMLES) model are investigated. Flow calculations are performed with OpenFOAM. Turbulent channel flow at various Reynolds number is considered.

Non-intrusive polynomial chaos is used to propagate the uncertainty in the closure coefficients. DAKOTA is used to calculate the Sobol Indices which quantify the sensitivity of each coefficient to some physical quantity of interest. The main quantity of interest in channel flow is the coefficient of skin friction. Details of the two LES models, the flow solver, and the test case are given in the following sections. Results and discussions of the UQ analyses are presented. Closure coefficients of interest are identified.

1.2 Brief Review of Literature

1.2.1 Large Eddy Simulation (LES)

Most naturally occurring flows in real world are turbulent. Their simulation using the computational fluid dynamics (CFD) requires accurately modeling of turbulence. Unfortunately,

the computation of turbulence flows from first principles by Direct Numerical Simulation (DNS) of Navier-Stokes equations is currently not feasible at high Reynolds numbers because of the requirements of computational power, which is unlikely to be available in the foreseeable future. Therefore, turbulent flows are generally modeled employing the Reynolds-Averaged Navier-Stokes (RANS) equations or Large-Eddy-Simulation (LES). Both approaches require a turbulence model. In this thesis, the focus is on LES.

In LES, the large-scale motions in turbulent flow are solved by modified form of Navier-Stokes equations but the small scale eddies (sub-grid scale (SGS) eddies) require modeling. The most well-known model for modeling the SGS eddies is the Smagorinsky model [1]. LES substantially reduces the computational intensity compared to DNS and is more accurate than the RANS approach wherein the entire turbulence flow field is modeled using a turbulence model.

1.2.2 Uncertainty Quantification (UQ)

There are always differences between the computed results and the real world experimental data. Errors in the simulation results occur due to the approximations in modeling as well as due to uncertainty in numerical solution process. It is important to know which parameters in the physical and numerical model contribute most to the uncertainty. The uncertainties can be classified into two categories [2]:

a. Aleatoric uncertainty or "irreducible" uncertainty

b. Epistemic uncertainty or "reducible" uncertainty

Aleatoric uncertainty is endogenous to the formulation; it represents the "known unknowns". Epistemic uncertainty arises from lack of knowledge; this type of uncertainty is the focus of this thesis.

In CFD, the flow simulations are very sensitive to physical model and numerical parameters, such as the computational mesh, numerical algorithm turbulence model etc. In the AIAA CFD drag prediction workshops [3-7], it has been shown that the numerical parameters such as the quality of mesh, the order of the numerical scheme and turbulence model significantly influence the results. The focus of this thesis is on uncertainty quantification of different coefficients in the LES models and based on UQ analysis, these coefficients are modified to improve the prediction capability of these models.

1.3 UQ Software

The DAKOTA toolbox is used for UQ, it provides an adaptable and extensible interface between the simulation codes and an iterative framework consisting of several examination techniques. DAKOTA contains calculation methods for advancement with inclination and nongradient-based strategies; uncertainty quantification with testing, dependability, stochastic extension, and epistemic techniques; parameter estimation with nonlinear slightest squares techniques; and affectability/fluctuation examination with plan of analyses and parameter contemplate techniques.

1.4 Flow Simulation Software

OpenFOAM is a free, open source software released and developed primarily by OpenCFD Ltd. since 2004. It has a broad popularity base across the world. OpenFOAM has an extensive range of features to solve complex fluid flow problems involving chemical reactions, turbulence and heat transfer, as well as for solution of acoustics, solid mechanics and electromagnetics problems.

In the OpenFOAM, a solver called pimpleFoam is used in this thesis. It is applied to LES of incompressible turbulent flow in a channel at various Reynolds numbers.

3

Chapter 2: Review of Uncertainty Quantification (UQ) and Large Eddy Simulation (LES)

2.1 Introduction to Uncertainty Quantification (UQ)

In this review of UQ, the Quadrature-Based Non-Intrusive Polynomial Chaos (NIPC) theory is utilized. In the context of UQ, NIPC can transform an irregular random variable into separable stochastic and deterministic parts as shown in Eq. (1), where $\alpha*$ could be any stochastic variable of interest, for example, pressure or skin friction coefficient, lift or drag coefficient, or any other time-averaged value in a turbulent fluid flow problem.

$$\alpha^*(t,\vec{x},\vec{\xi}) \approx \sum_{j=0}^{P} \alpha_j(t,\vec{x})\Psi_j(\vec{\xi}) \tag{1}$$

In Eq. (1), $\Psi_j(\vec{\xi})$ is the stochastic basis function with respect to the mode of order j. $\alpha*$ is an element of the free deterministic variable vector $(t,\vec{x})$ and the n-dimensional random variable vector $\vec{\xi} = (\xi_1, \dots, \xi_n)$; both aleatory and epistemic uncertain factors are incorporated into this condition. In this formulation, the polynomial chaos expansion (PCE) method is used since Eq. (1) ought to have boundless number of terms; however a discrete summation is assumed. To achieve an expansion of order p, the aggregate number of cases (N_t) is given by the Eq. (2):

$$N_t = P + 1 = n_p \frac{(n+p)!}{n!\,p!} \tag{2}$$

As shown in Eq. (2) N_t is a function of number of random dimensions (n) and the order of PCE (p). When the input uncertainty is Gaussian, the basis function can be a multi-dimensional Hermite Polynomial to develop the n-dimensional stochastic space, which was initially proposed by Wiener [8] in his paper on polynomial chaos. To promote the use of the polynomial chaos hypothesis, an

arrangement of polynomials was utilized by Xiu and Karniadakis [9] as an Askey scheme to develop the Wiener-Askey Generalized Polynomial Chaos. The weight and density functions for few of the most widely used polynomials are shown in Table 2.1. As described in the review by Huyse et al. [10], the Hermite, Legendre and Laguerre polynomials are three most widely used basis functions.

Table 2.1 Density and Weight Functions of Commonly Used Univariate Optimal Basis Functions.

Input Distribution	Density Function	Polynomial Name	Weight Function	Support Range (R)
Normal	$\frac{1}{\sqrt{2\pi}}e^{\frac{-\xi^2}{2}}$	Hermite, $H_n(\xi)$	$e^{\frac{-\xi^2}{2}}$	$[-\infty, \infty]$
Uniform	$\frac{1}{2}$	Legendre, $Le_n(\xi)$	1	$[-1,1]$
Exponential	$e^{-\xi}$	Laguerre, $La_n(\xi)$	$e^{-\xi}$	$[0, \infty]$

For an input uncertainty variable, there are three types of distribution called the Gaussian (typical), bounded (uniform) and semi-bounded (exponential). The ideal basis functions are the result of the weight functions multiplied by the standard probability density functions (PDF) of a known input uncertainty variable. The standard PDF must achieve the basic condition that the integration of the PDF over the whole range reaches a finite value. A direct consequence of this requirement is the multiplication between the density function and weight function which appear in Table 2.1. When there are more than one uncertainty variables, the multivariate basis functions can be obtained from orthogonal polynomials, as described in Eldred et al. [11]. For example, a multivariate Hermite polynomial can be obtained as

$$H_n(\xi_{i1}, \dots, \xi_{in}) = H_n(\vec{\xi}) = e^{\frac{1}{2}\vec{\xi}^T\vec{\xi}}(-1)^n \frac{\partial^n}{\partial \xi_{i1}, \dots, \xi_{in}} e^{-\frac{1}{2}\vec{\xi}^T\vec{\xi}} \qquad (3)$$

5

Eq. (3) can also be obtained from one-dimensional Hermite Polynomials $\psi_{m_i^j}(\xi_i)$ by using the

multi-index m in another form as shown in Eq. (4):

$$H_n(\xi_{i1}, \dots , \xi_{in}) = \Psi_j(\vec{\xi}) = \prod_{i=1}^{n} \psi_{m_i^j}(\xi_i) \tag{4}$$

The fundamental data of the polynomial chaos strategy is to decide the coefficients in Eq. (1). At

that point, the significance of how the information impacts the result can be ascertained by utilizing

the p basis functions and these coefficients.

For example, Hosder et al. [12] have demonstrated that the mean value of a stochastic function is

given by

$$\mu_{\alpha^*} = \vec{\alpha}^*(t, \vec{x}) = E_{PC}\left(\alpha^*(t, \vec{x}, \vec{\xi})\right) = \int_R \alpha^*(t, \vec{x}, \vec{\xi})p(\vec{\xi})d\vec{\xi} = \alpha_0(t, \vec{x}) \tag{5}$$

Eq. (5) gives the expected or mean value of the output $\alpha^*(t, \vec{x}, \vec{\xi})$, it is simply the zeroth coefficient

of the polynomial chaos expansion. Hosder et al. [12] show that there is an expression for changing

the range of the output:

$$\mu_{\alpha^*}^2 = \int_R \left(\alpha^*(t, \vec{x}, \vec{\xi}) - \overline{\alpha_0^*}(t, \vec{x})\right)^2 p(\vec{\xi})d\vec{\xi} = \sum_{j=1}^{P} [\alpha_j^2 \langle \Psi_j^2 \rangle] \tag{6}$$

Equations (5) and (6) employ the fact that $\langle \Psi_i \Psi_j \rangle = \langle \Psi_j \rangle \delta_{ij}$ and $\langle \Psi_j \rangle = 0$ for $j > 0$, where δ_{ij} is

the Kronecker delta function. The dot product of $\Psi_i(\vec{\xi})$ and $\Psi_j(\vec{\xi})$ over the range R is defined as:

$$\langle \Psi_i(\vec{\xi})\Psi_j(\vec{\xi}) \rangle = \int_R \Psi_i(\vec{\xi})\Psi_j(\vec{\xi})p(\vec{\xi})d\vec{\xi} \tag{7}$$

where $p(\vec{\xi})$ is the probability density function.

In the event that the probability distribution of every stochastic variable is distinctive, the ideal

multivariate basis functions can be obtained from the product of univariate quadrature polynomials

utilizing the ideal univariate polynomial in each stochastic dimension. In this strategy, it is required

that the uncertainties utilized as input are independent typical stochastic factors. More insights about the polynomial chaos expansion can be found in the papers of Walters and Huyse [13], Najm [14], and Hosder and Walters [12]. Typically, two types of polynomial chaos, intrusive and non-intrusive are utilized for the uncertainty quantification in computational reproduction. Although straightforward in theory, an intrusive formulation for complex problems can be somewhat difficult and costly, and requires more resources to accomplish.

To overcome the disadvantages of the intrusive approach, non-intrusive polynomial chaos (NIPC) formulations is chosen for uncertainty quantification in this study.

2.2 Large Eddy Simulation (LES)

Large eddy simulation (LES) is a well-known model for simulating turbulent flows. A theory developed by Kolmogorov in 1941 showed that the large eddies in a turbulent flow are dependent on the geometry while the smaller eddies are universal. This concept was used in the formulation of LES model from the Navier-Stokes euqations.

In LES, the small-scale eddies near the wall of a turbulent boundary layer for example are modeled while the large scale eddies away from the wall are calculated directly by the Navier-Stokes equations. To accomplish this, filtering is performed. Filtering is defined as the convolution of a function u with a filtering kernel G:

$$\bar{u}_i(\vec{x}) = \int G\left(\vec{x} - \vec{\bar{\xi}}\right) u(\vec{\bar{\xi}}) \mathrm{d}\vec{\bar{\xi}} \tag{8}$$

It results in

$$u_i = \bar{u}_i + u_i' \tag{9}$$

where $\bar{u}_i$ is the resolvable large scale part and u_i' is the subgrid-scale part of variable u. However, most practical implementations of LES utilize the computational grid as the filter (the box filter) and do not employ explicit filtering.

The filtered equations can be obtained from the incompressible Navier-Stokes equations given below:

$$\frac{\partial u_i}{\partial t} + u_j \frac{\partial u_i}{\partial x_j} = -\frac{1}{\rho}\frac{\partial p}{\partial x_i} + \frac{\partial}{\partial x_i}\left(v\frac{\partial u_i}{\partial x_j}\right) \tag{10}$$

Substituting $u_i = \bar{u}_i + u_i'$ and $p = \bar{p} + p'$ in Eq. (10) and then filtering the resulting equation using Eq. (8) results in the equation for the resolved field:

$$\frac{\partial \bar{u}_i}{\partial t} + \bar{u}_j \frac{\partial \bar{u}_i}{\partial x_j} = -\frac{1}{\rho}\frac{\partial \bar{p}}{\partial x_i} + \frac{\partial}{\partial x_i}\left(v\frac{\partial \bar{u}_i}{\partial x_j}\right) + \frac{1}{\rho}\frac{\partial \tau_{ij}}{\partial x_j} \tag{11}$$

The new term $\frac{\partial \tau_{ij}}{\partial x_j}$ in Eq. (11) arises from the non-linear advection terms since

$$\overline{u_j \frac{\partial u_i}{\partial x_j}} \neq \bar{u}_j \frac{\partial \bar{u}_i}{\partial x_j} \tag{12}$$

Therefore,

$$\tau_{ij} = \bar{u}_i \bar{u}_j - \overline{u_i u_j} \tag{13}$$

Similar equations can be derived for the subgrid-scale field.

Boussinesq hypothesis is used in subgrid-scale (SGS) modeling of turbulence. The SGS turbulent stress can be modeled as:

$$\tau_{ij} - \frac{1}{3}\tau_{kk}\delta_{ij} = -2\mu_t \bar{S}_{ij} \tag{14}$$

where $\bar{S}$ is the strain-rate tensor for the resolved scale defined as:

$$\bar{S}_{ij} = \frac{1}{2}\left(\frac{\partial \bar{u}_i}{\partial x_j} + \frac{\partial \bar{u}_j}{\partial x_i}\right) \tag{15}$$

In Eq. (14), μ_t is the subgrid-scale turbulent eddy viscosity. Employing Eqs. (11) - (15), the Navier-Stokes equations become:

$$\frac{\partial \bar{u}_i}{\partial t} + \bar{u}_j \frac{\partial \bar{u}_i}{\partial x_j} = -\frac{1}{\rho}\frac{\partial \bar{p}}{\partial x_i} + \frac{\partial}{\partial x_i}\left([v + v_t]\frac{\partial \bar{u}_i}{\partial x_j}\right) \tag{16}$$

where the incompressibility constraint has been used to simplify the equation and the pressure is modified to include the trace term $\tau_{kk}\delta_{ij}/3$.

2.2.1 Smagorinsky Model

In order to close the equations and determine the filtered velocity field $\bar{u}(x,t)$ and the filtered pressure $\bar{p}(x,t)$, one needs to model the anisotropic residual-stress tensor $\tau_{ij}^r(x,t)$. The Smagorinsky model is the simplest model which has been proven to perform reasonably well. In this model, the residual subgrid-scale eddy viscosity v_t is modeled to represent the motion of subgrid scale eddies. v_t is modeled as:

$$v_t = l_s^2(2\overline{S_{lk}S_{lk}})^{\frac{1}{2}} = (C_s\Delta)^2(2\overline{S_{lk}S_{lk}})^{\frac{1}{2}} \tag{17}$$

where the Smagorinsky length scale is defined by $l_s = C_s\Delta$, where C_s is the Smagorinsky coefficient and Δ is the filter width. The filtered Navier-Stokes equations can be written as:

$$\partial_t\overline{u_j} + \overline{u_i}\partial_t\overline{u_j} = 2\partial_i\left(\left(v + l_s^2(2\overline{S_{lk}S_{lk}})^{\frac{1}{2}}\right)\overline{S}_{ij}\right) - \partial_j\bar{p} + \overline{f_j}, \qquad j = 1,2,3 \tag{18}$$

In OpenFOAM the Smagorinsky coefficient C_s is calculated by two coefficients which are named C_k and C_ε. The relationship between C_s and C_s, C_ε can be written as:

$$(C_s)^2 = C_k\sqrt{\frac{C_k}{C_\varepsilon}} \tag{19}$$

The model constants and their recommended bounds are given in Table 2.2. These bounds were determined based on the behavior of the model when applied to canonical free shear flows and a turbulent boundary layer.

Table 2.2 Epistemic Intervals of Closure Coefficients for Smagorinsky model.

Closure Coefficient	Lower Bound	Upper Bound	Standard Value
C_ε	0.984	1.152	1.048
C_k	0.085	0.103	0.094

2.2.2 Wall-Modeled Large Eddy Simulation (WMLES)

The equilibrium wall-model used in this study is given by

$$\frac{\partial}{\partial y}\left[(\mu + \mu_t)\frac{\partial u}{\partial y}\right] = 0$$

$$\frac{\partial}{\partial y}\left[(\mu + \mu_t)u\frac{\partial u}{\partial y} + c_p\left(\frac{\mu}{Pr} + \frac{\mu_t}{Pr_t}\right)\frac{\partial T}{\partial y}\right] = 0 \tag{20}$$

The WMLES model is more complex than the Smagorinsky model since it includes the modeling of sublayer. In the sublayer, ν_t can be expressed by the van Driest equation:

$$\nu_t = \kappa y\sqrt{\frac{\tau_w}{\rho}}\left[1 - \exp\left(\frac{y^+}{A^+}\right)\right]^2 \tag{21}$$

Thus, the modified Smagorinsky model becomes:

$$\nu_t = \min\{(\kappa y)^2, (C_s\Delta)^2\}\left[1 - \exp\left(\frac{y^+}{A^+}\right)\right]^2 \tag{22}$$

The model constants for WMLES model and their recommended bounds are shown in Table 2.3. These bounds were determined based on the behavior of the model when applied to canonical free shear flows and a turbulent boundary layer.

Table 2.3 Epistemic Intervals of Closure Coefficients for WMLES model.

Closure Coefficient	Lower Bound	Upper Bound	Standard Value
C_ε	0.984	1.152	1.048
C_k	0.085	0.103	0.094
κ	0.369	0.451	0.41
A^+	23.4	28.6	26

Chapter 3: Validation of LES Result

In this chapter, LES results are compared with the DNS data to assess their accuracy. The implementations of the Smagorinsky model and WMLES model are verified by the comparing LES simulations against the DNS data for turbulent flow in a channel.

3.1   Comparison of Velocity Profiles at $Re_\tau = 395$
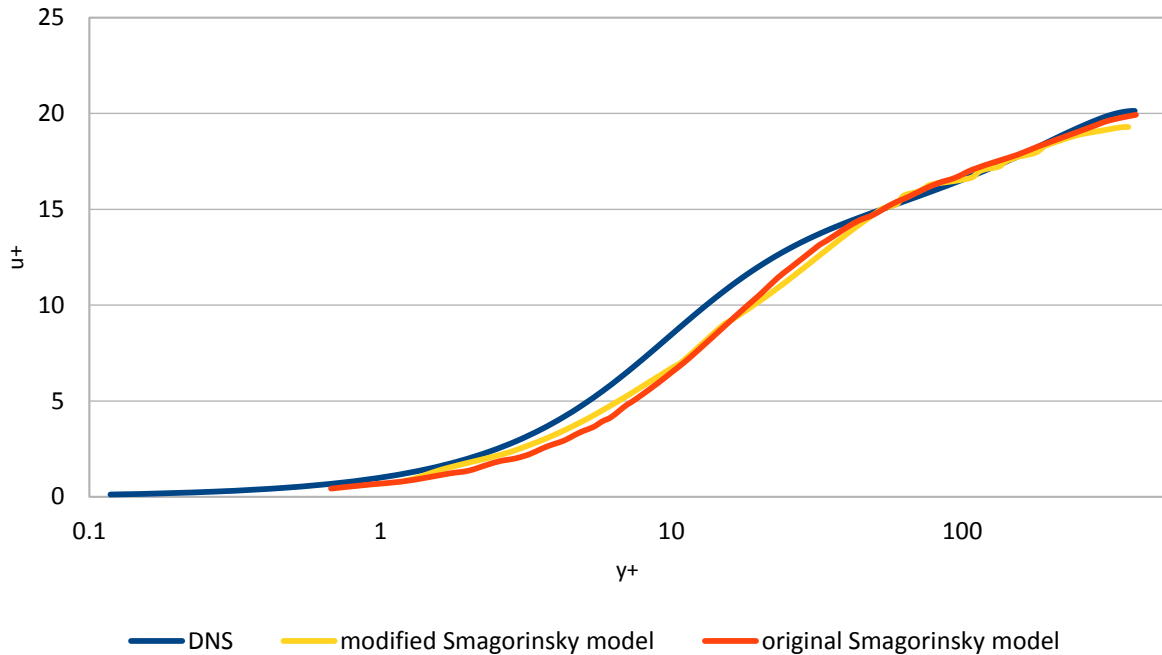
Figure 3.1 Comparison of velocity profiles for fully developed turbulent flow in a channel using the LES with original Smagorinsky model [1], the modified Smagorinsky model [15] and DNS [16] at $Re_\tau = 395$

In Fig. 3.1, the fully developed velocity profiles at $Re_\tau = 395$ are presented using the original Smagorinsky model [1] and the modified Smagorinsky model [15] and are compared with the DNS data [16]. The maximum velocity at the center of the channel from experimental data is 1.15m/s, from original Smagorinsky model is 1.227m/s and from modified Smagorinsky model is 1.196m/s.

As can be seen, the two LES simulations are in close agreement with each other, however there is considerable difference in LES results against DNS data in the logarithmic region near the wall.

3.2 Comparison of Velocity Profiles at Re$_\tau$ = 550

In Fig. 3.2, the fully developed velocity profiles at Re$_\tau$ = 550 are presented using the Smagorinsky model and the WMLES model and are compared with the DNS data [16]. The maximum velocity at the center of the channel from experimental data is 1.14m/s, from Smagorinsky model is 1.203m/s and from WMLES model is 1.196m/s. As can be seen, result from WMLES model is more accurate than that from the Smagorinsky model, and there is considerable difference in LES results against DNS data in the logarithmic region near the wall.
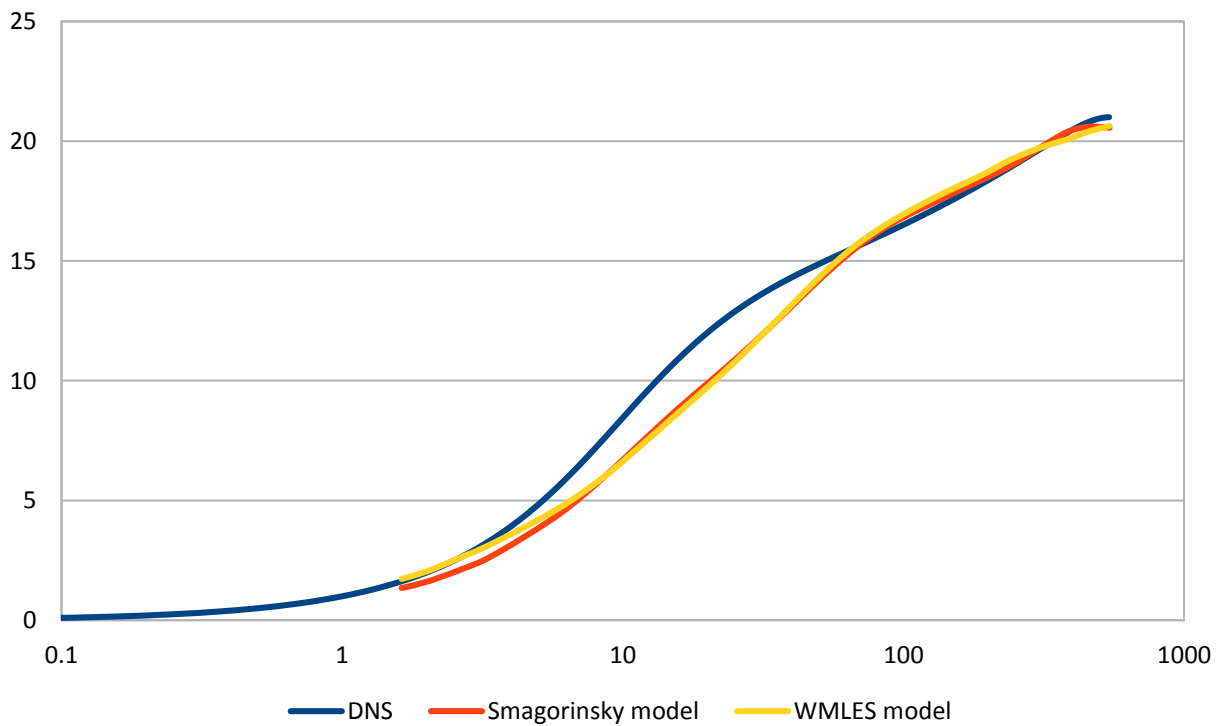
Figure 3.2 Comparison of velocity profiles for fully developed turbulent flow in a channel using the LES with the Smagorinsky model, the WMLES model and DNS [16] at Re$_\tau$ = 550.

3.3　Comparison of Velocity Profiles at $Re_\tau = 2000$

In Fig. 3.3, the fully developed velocity profiles at $Re_\tau = 2000$ are presented using the Smagorinsky model and the WMLES model and are compared with the DNS data [16]. The maximum velocity at the center of the channel from experimental data is 1.158m/s, from Smagorinsky model is 1.135m/s and from WMLES model is 1.149m/s. As can be seen, result from WMLES model is more accurate than that from the Smagorinsky model, and there is considerable difference in LES results against DNS data in the logarithmic region near the wall.
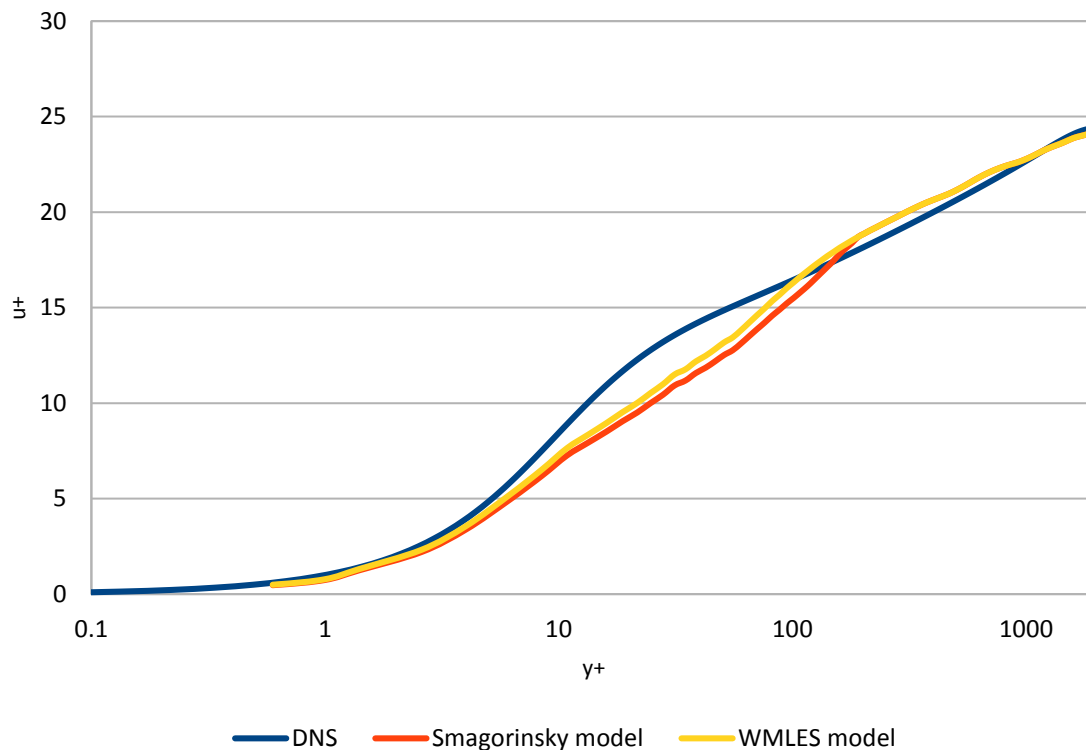
Figure 3.3 Comparison of velocity profiles for fully developed turbulent flow in a channel using the LES with the Smagorinsky model, the WMLES model and DNS [16] at $Re_\tau = 2000$

3.4   Comparison of Velocity Profiles at $Re_\tau = 5200$

In Fig. 3.4, the fully developed velocity profiles at $Re_\tau = 5200$ are presented using the Smagorinsky model and the WMLES model and are compared with the DNS data [16]. The maximum velocity at the center of the channel from experimental data is 1.151m/s, from Smagorinsky model is 1.102m/s and from WMLES model is 1.139m/s. As can be seen, result from WMLES model is more accurate than that from the Smagorinsky model, and there is considerable difference in LES results against DNS data in the logarithmic region near the wall.
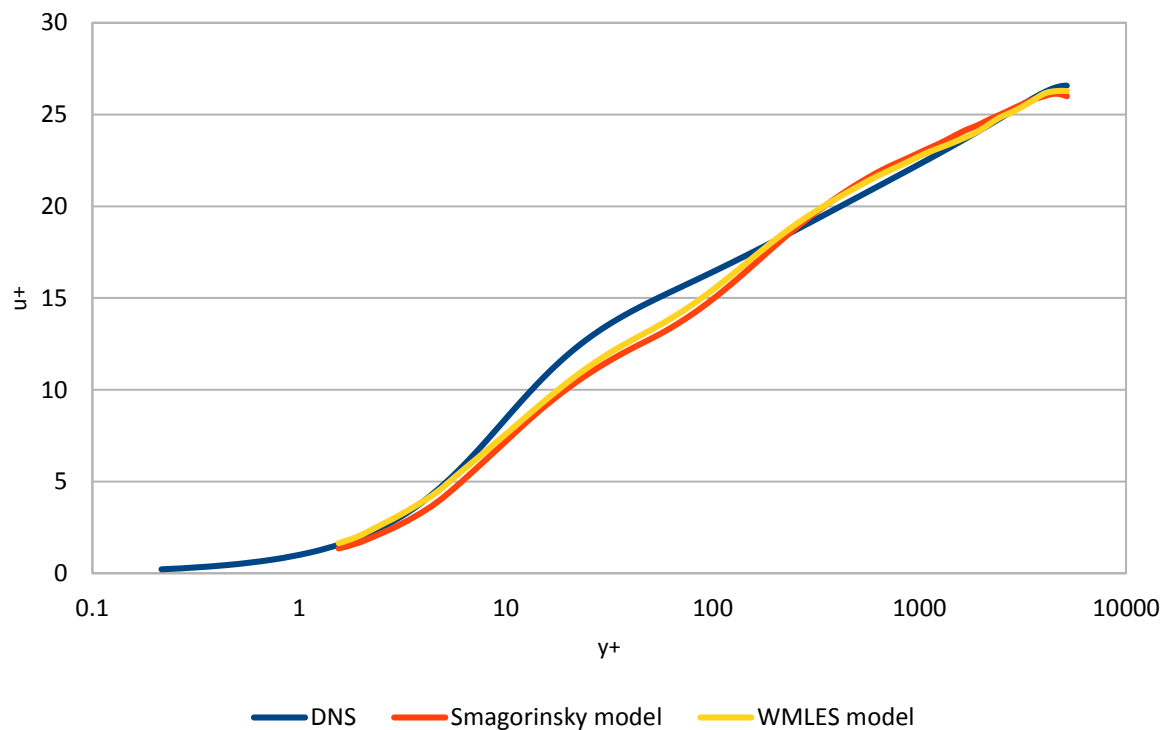
Figure 3.4 Comparison of velocity profiles for fully developed turbulent flow in a channel using the LES with the Smagorinsky model, the WMLES model and DNS [16] at $Re_\tau = 5200$

15

3.5   Conclusions

It can be calculated from the results presented in the chapter that there is considerable difference between the DNS data and LES result at various Reynolds numbers for turbulent flow in a channel. However, at all Reynolds number considered, the WMLES result are always slightly more accurate than that from the Smagorinsky model. The reason is that WMLES model is more accurate than the Smagorinsky model in the sublayer near the wall.

Chapter 4: Mesh and Boundary Conditions

The fully developed turbulent channel flow is a widely used simple verification and validation test case for various simulation models namely RANS, LES and DNS. The Reynolds numbers of the flow considered in this thesis are Re_τ = 395, 550, 2000 and 5200. The computational grids employed are taken from the tutorial for turbulent channel flow at Re_τ = 395 in OpenFOAM. The computational grid with every other node and boundary conditions for various Reynolds numbers are shown in Figs. 4.1 – 4.4. The case of Re_τ = 395 is used to determine the sensitivities of the model coefficients for Smagorinsky and WMLES using UQ in code DAKOTA.

4.1   Mesh and Boundary Conditions at Re_τ = 395

At Re_τ = 395, mesh is set at 40*25*30, with a total of 30000 cells. For the boundary named topWall and bottomWall, the boundary condition is set as no slip. The other boundaries, are set as periodic or cyclic, in the two directions X and Y.
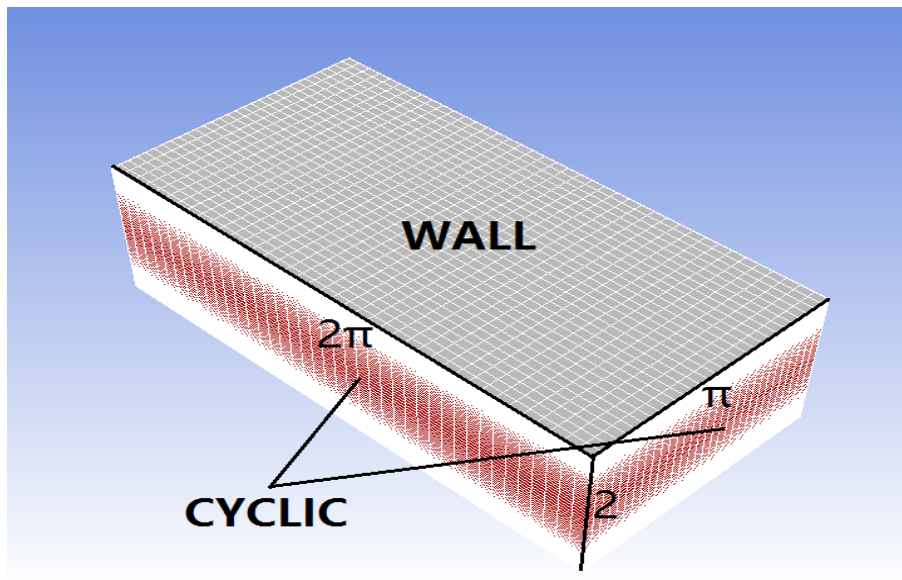
Figure 4.1 Mesh and boundary conditions at Re_τ = 395

17

4.2 Mesh and Boundary Conditions at Re$_\tau$ = 550
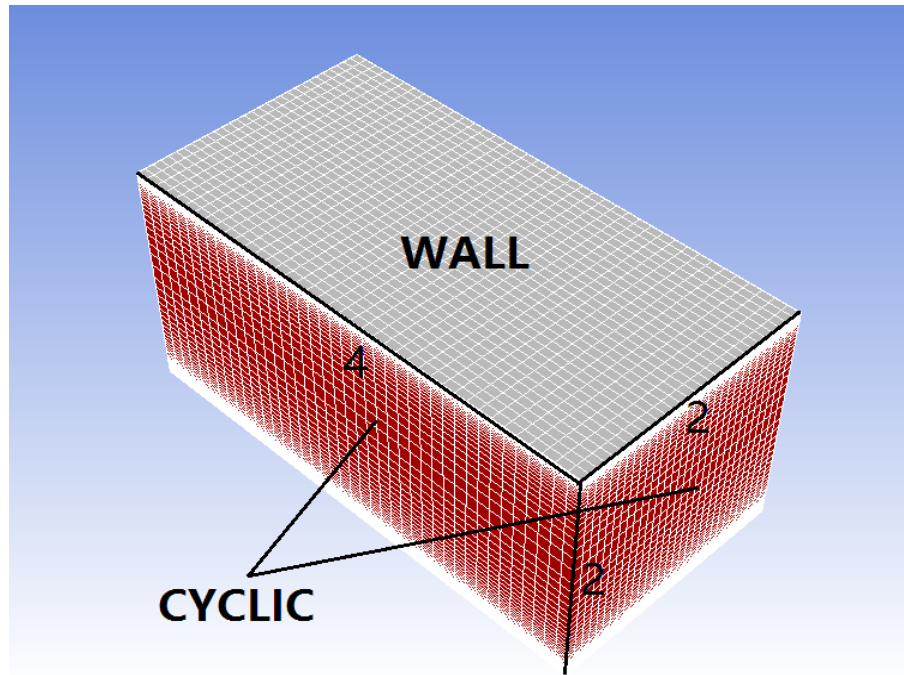
Figure 4.2 Mesh and boundary conditions at Re$_\tau$ = 550

At Re$_\tau$ = 550, mesh is set at 40*50*30, with a total of 60000 cells. For the boundary named topWall and bottomWall, the boundary condition is set as no slip. The other boundaries, are set as periodic or cyclic, in the two directions X and Y.

4.3 Mesh and Boundary Conditions at Re$_\tau$ = 2000

At Re$_\tau$ = 2000, mesh is set at 40*100*30, with a total of 120000 cells. For the boundary named topWall and bottomWall, the boundary condition is set as no slip. The other boundaries, are set as periodic or cyclic, in the two directions X and Y.
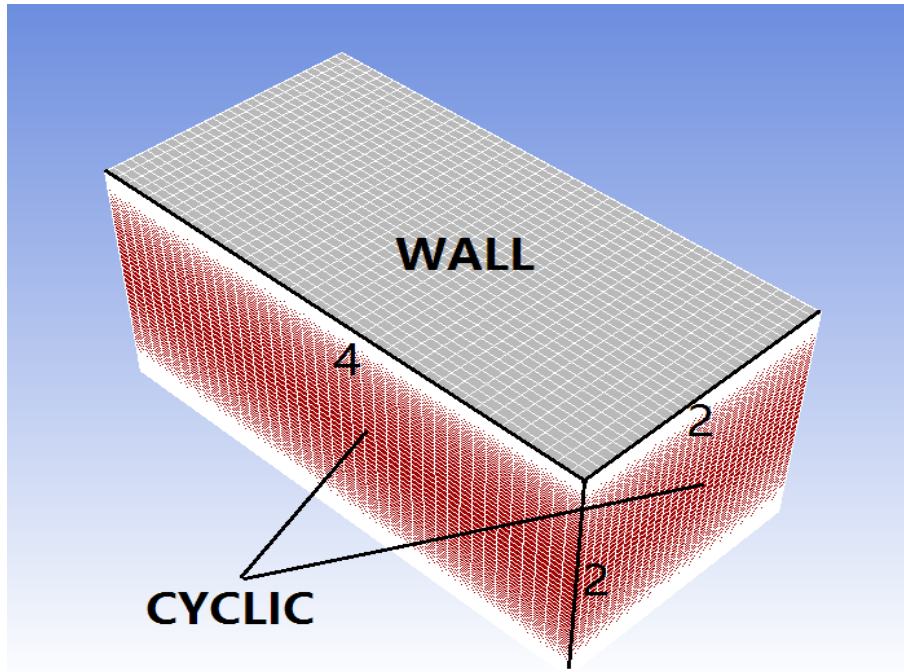
Figure 4.3 Mesh and boundary conditions at Re$_\tau$ = 2000

4.4 Mesh and Boundary Conditions at Re$_\tau$ = 5200

At Re$_\tau$ = 5200, mesh is set at 80*100*60, with a total of 480000 cells. For the boundary named topWall and bottomWall, the boundary condition is set as no slip. The other boundaries, are set as periodic or cyclic, in the two directions X and Y.
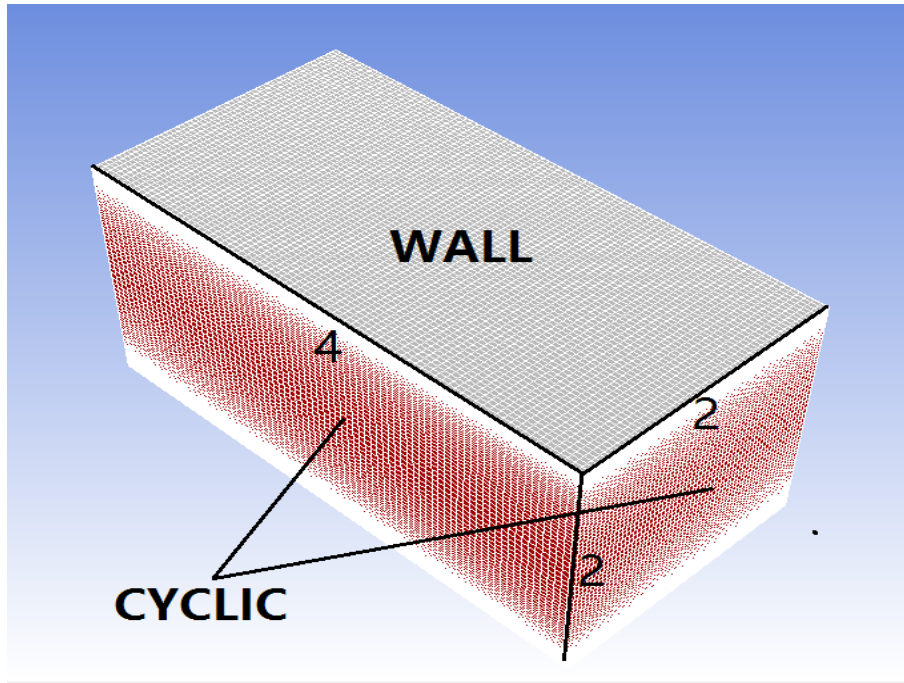
Figure 4.4 Mesh and boundary conditions at Re$_\tau$ = 5200

Chapter 5: UQ of Skin Friction Coefficient with Smagorinsky and WMLES models

5.1 Sobol Indices for Skin Friction Coefficient

Tables describe the sensitivity of the LES turbulence models (Smagorinsky and WMLES) to changes in the model's closure coefficients for the channel flow at different Reynolds numbers. OpenFOAM is used as the flow solver and Sobol indices, are computed using SANDIA National Labs DAKOTA software; Sobol indices are used to rank the influence of each model coefficient. Tables 5.1 – 5.3 show the sensitivity analysis results obtained from OpenFOAM for the skin friction coefficients at $Re_\tau = 550$, $Re_\tau = 2000$ and $Re_\tau = 5200$.

5.1.1 Sobol Indices for $Re_\tau = 550$

Table 5.1 Sobol Indices for the skin friction coefficient from OpenFOAM when $Re_\tau = 550$.

Smagorinsky		WMLES	
Coefficient	Sobol Index	**Coefficient**	Sobol Index
C_k	0.693	C_k	0.380
C_ε	0.307	C_ε	0.302
		κ	0.216
		A^+	0.102

As shown in Table 5.1, for $Re_\tau = 550$, in Smagorinsky model there are only two coefficients. Between C_k and C_ε, the most significant coefficient is obviously C_k, which has a Sobol index of 0.693; C_ε has a index of 0.307. C_k also plays an important role in case of WMLES model. However, C_ε.also contributes significantly in case of WMLES model. Coefficients κ and A^+ do not appear

to be very important in WMLES model at $Re_\tau = 550$, the sum of their Sobol Indices is only 0.318, less than that of C_k.

5.1.2 Sobol Indices for $Re_\tau = 2000$

Table 5.2 Sobol indices for the skin friction coefficient from OpenFOAM when $Re_\tau = 2000$

Smagorinsky		WMLES	
Coefficient	Sobol Index	**Coefficient**	Sobol Index
C_k	0.543	C_k	0.104
C_ε	0.457	C_ε	0.077
		κ	0.501
		A^+	0.318

As shown in Table 5.2, at $Re_\tau = 2000$, in case of Smagorinsky model, the most significant coefficient is C_k, although it begins to decrease compared to $Re_\tau = 550$ case, its significance is still higher than that of C_ε. In case of WMLES model, the coefficient which contributes most to the skin friction coefficient is κ with Sobol index of 0.501. A^+ also has an index of 0.318. The Sobol indices are completely different with case compared to those for $Re_\tau = 550$. C_ε and C_k become less important in WMLES model when $Re_\tau = 2000$.

5.1.3 Sobol Indices for $Re_\tau = 5200$

At $Re_\tau = 5200$, in Smagorinsky model, the most significant coefficient is C_ε, with a Sobol index of 0.652, completely opposite to the situation for $Re_\tau = 550$ case. In case of WMLES model, the coefficient which contributes most to the skin friction coefficient is A^+. κ also has an important influence on the result with a Sobol index of 0.339. C_ε and C_k become least important most in case of WMLES model at $Re_\tau = 5200$, with Sobol index of 0.107 and 0.068, respectively.

Table 5.3 Sobol indices for the skin friction coefficient from OpenFOAM when Re$_\tau$ = 5200.

Smagorinsky		WMLES	
Coefficient	Sobol Index	**Coefficient**	Sobol Index
C_k	0.348	C_k	0.068
C_ε	0.652	C_ε	0.107
		κ	0.339
		A^+	0.486

5.2 Change in Skin Friction Coefficient with Change in Coefficients of Smagorinsky and WMLES model

5.2.1 Change in Skin Friction Coefficient in Smagorinsky Model

Table 5.4 – 5.7 show two change in skin-friction by changing the coefficients (decreasing and increasing by 10% from the standard value) in Smagorinsky and WMLES models.

Table 5.4 Sobol indices at various Re$_\tau$ for Smagorinsky model by decreasing the coefficients by 10%.

Coefficient	Smagorinsky					
	Re$_\tau$ = 550		**Re$_\tau$ = 2000**		**Re$_\tau$ = 5200**	
	C_f	%change	C_f	%change	C_f	%change
C_{k-}	4.456E-03	-1.81%	3.318E-03	-1.31%	2.804E-03	-1.02%
$C_{\varepsilon-}$	4.587E-03	1.08%	3.399E-03	1.07%	2.898E-03	2.29%

Table 5.5 Sobol indices of for various Re$_\tau$ for Smagorinsky model with increasing coefficients by 10%.

Coefficient	Smagorinsky					
	Re$_\tau$ = 550		**Re$_\tau$ = 2000**		**Re$_\tau$ = 5200**	
	C_f	%change	C_f	%change	C_f	%change
C_{k+}	4.644E-03	2.33%	3.435E-03	2.17%	2.869E-03	1.27%
$C_{\varepsilon+}$	4.499E-03	-0.86%	3.318E-03	-1.31%	2.759E-03	-2.61%

It can be seen from Table 5.4 – 5.7 that in case of Smagorinsky model, as coefficients increased by 10%, skin friction coefficient increases with C_k, but decreases with C_ε. Similar situation occurs when the coefficients decrease by 10%.

5.2.2 Change in Skin Friction Coefficient in WMLES Model

Table 5.6 Sobol indices at various Re$_\tau$ for WMLES model by decreasing the coefficients by 10%.

Coefficient	WMLES					
	Re$_\tau$ = 550		**Re$_\tau$ = 2000**		**Re$_\tau$ = 5200**	
	C_f	%change	C_f	%change	C_f	%change
C_{k-}	4.410E-03	-2.82%	3.331E-03	-0.92%	2.810E-03	-0.81%
$C_{\varepsilon-}$	4.642E-03	2.29%	3.383E-03	0.62%	2.869E-03	1.27%
κ_-	4.459E-03	-1.74%	3.303E-03	-1.75%	2.782E-03	-1.80%
A^+_-	4.507E-03	-0.68%	3.312E-03	-1.49%	2.726E-03	-3.78%

Table 5.7 Sobol indices at various Re$_\tau$ for WMLES model by increasing coefficients by 10%

Coefficient	WMLES					
	Re$_\tau$ = 550		**Re$_\tau$ = 2000**		**Re$_\tau$ = 5200**	
	C_f	%change	C_f	%change	C_f	%change
C_{k+}	4.646E-03	2.38%	3.387E-03	0.71%	2.861E-03	0.99%
$C_{\varepsilon+}$	4.451E-03	-1.92%	3.346E-03	-0.51%	2.791E-03	-1.48%
κ_+	4.610E-03	1.59%	3.450E-03	2.59%	2.899E-03	2.33%
A^+_+	4.587E-03	1.08%	3.427E-03	1.90%	2.923E-03	3.17%

In case of WMLES model, it can be seen from Table 5.6 and 5.7 that when the coefficients increase by 10%, skin friction coefficient increases with C_k, κ and A^+ but decreases with C_ε. Similar situation occurs when the coefficients decrease by 10%.

5.3 Conclusions

Several interesting conclusions can be made from the result in section 5.2.

First, in case of Smagorinsky model, the sensitivity of C_k decreases and that of C_ε becomes more important, with increasing Reynolds number. Also, as the Reynolds number becomes larger, C_k and C_ε reverse the role in terms of importance.

In case of WMLES model, sensitivity of different model coefficients on the skin-friction coefficient change with Reynolds number. With increase in Reynolds number, importance of C_k and C_ε on the skin friction coefficient becomes less and less, and that of κ and A^+ becomes more. Table 5.8 and 5.9 show the Sobol indices in two model coefficients in their overlapping region and variation in their value with Reynolds number.

Table 5.8 Sobol indices of a combination of two model coefficients for the skin friction coefficient from OpenFOAM for Smagorinsky model

Smagorinsky			
Coefficients Combination	**Sobol indices in the overlapping region**		
	Re$_\tau$ = 550	**Re$_\tau$ = 2000**	**Re$_\tau$ = 5200**
C_ε & C_k	1.97E-01	2.03E-02	6.75E-03

Table 5.9 Sobol indices of a combination of two model coefficients for the skin friction coefficient from OpenFOAM for WMLES model

WMLES			
Coefficients Combination	**Sobol indices in the overlapping region**		
	Re$_\tau$ = 550	**Re$_\tau$ = 2000**	**Re$_\tau$ = 5200**
C_ε & C_k	1.80E-01	2.71E-03	2.29E-03
C_ε & κ	2.86E-01	4.94E-02	9.10E-03
κ & C_k	2.20E-02	1.07E-02	1.25E-04
C_ε & A^+	2.17E-03	1.35E-03	1.06E-01

A^+ & C_k	1.30E-01	1.30E-02	4.54E-02
κ & A^+	1.31E-02	2.05E-01	2.44E-01

Chapter 6: UQ of Mean Velocity Profiles from Smagorinsky and WMLES Model

In this chapter, uncertainty quantification (UQ) of velocity profiles in the channel obtained using the Smagorinsky model and WMLES model is conducted. It will be shown how the model coefficients can influence the velocity profile at various Reynolds numbers. By changing the model coefficients, the sensitivity of the coefficients on the global velocity profile is also shown.

6.1 UQ of Velocity Profile when $Re_\tau = 550$

6.1.1 UQ of Velocity Profile from Smagorinsky Model

As shown in Fig.6.1, at $Re_\tau = 550$, for Smagorinsky model, the Sobol index of C_k begins around 0.748 and that of C_ε around 0.252. Sobol index of C_k reaches maximum value of 0.997 when y^+ is 100. After that, the Sobol index of C_k decreases, and remains near 0.7 when y^+ is between 175 and 350. When distance from the wall becomes large, C_k again dominates the change in and finally becomes 0.988 in the middle of the channel.

C_k can be regarded as the most significant coefficient in this case. If a more accurate prediction of velocity is required using the LES Smagorinsky model, the most effective way is to change C_k. After several computational tests, it can be found that as C_k is increased, velocity profile gets closer to the DNS data. As shown in Fig. 6.2, red lines and green lines are the velocity profiles when the that value of C_k increased by 20% and 10%, respectively with respect to their original value.
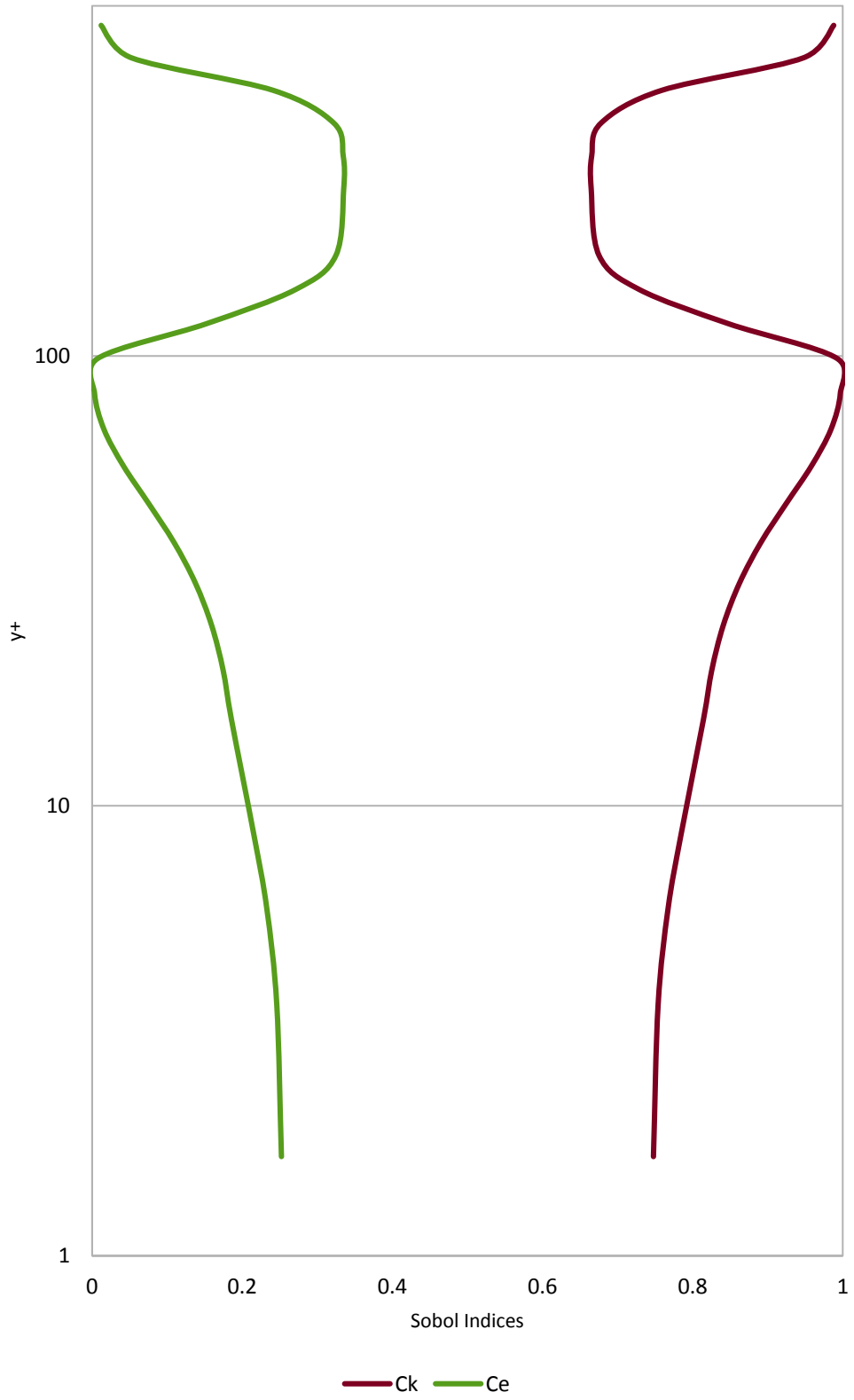
Figure 6.1 Sobol indices along the y direction for Smagorinsky model at Re$_\tau$ = 550
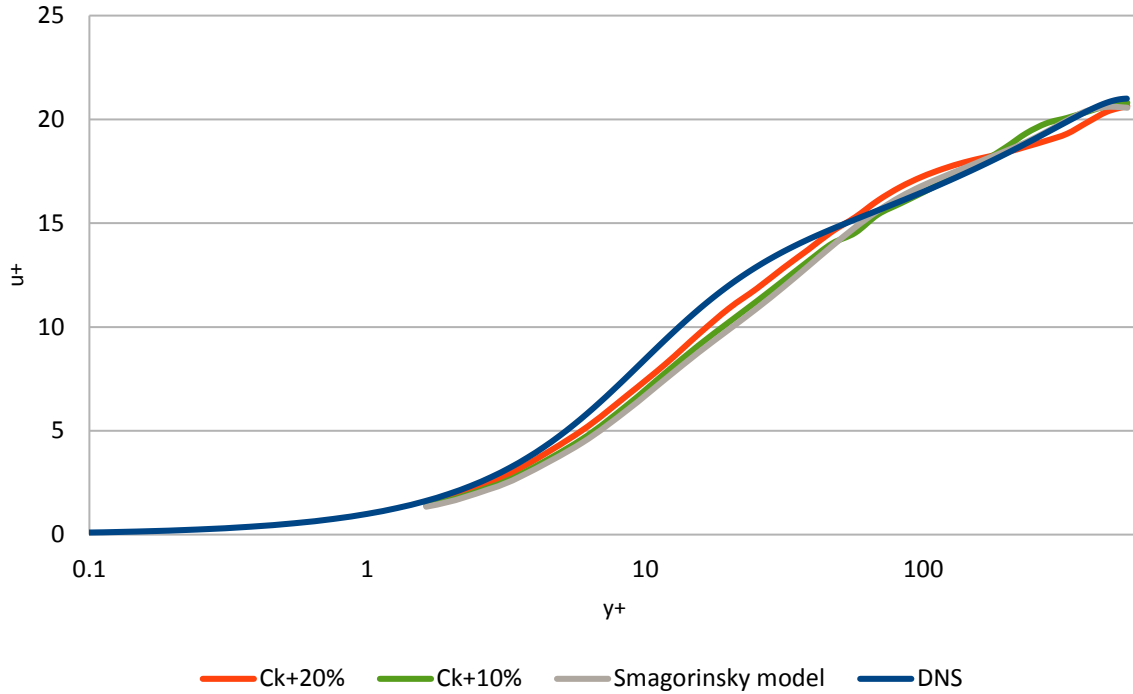
Figure 6.2 Comparison of velocity profiles obtained by increasing C_k by 20% and 10% for Smagorinsky model with DNS data at $Re_\tau = 550$

6.1.2 UQ of Velocity Profiles for WMLES Model

As shown in Fig. 6.3, The situation is more complex compared to that the situation for Smagorinsky model since there are four model coefficients. κ ranks first when y^+ begins to increase. Before y^+ reaches 100, κ is always the most influential coefficient in affecting the mean velocity. As y^+ becomes greater than 30, which is the log-law region, the coefficient C_ε begins to increase and becomes the most significant coefficient to affect the mean velocity after $y^+ = 100$. However, when y^+ is between 150 and 350, it can be seen from this figure that C_k most influences the mean velocity. Finally, near the middle of the channel, A^+ contributes most to the mean velocity profile.

κ is the most important coefficient in the buffer layer. After several computational tests, it was found that decreasing κ is the best way to make the velocity profile closer to the DNS data. In Fig.

29

6.4, it can be seen that by decreasing κ by 20% and 10%, velocity profile becomes closer to the DNS data.

Thus, it can be inferred that y^+ has an enormous influence on the value of Sobol indices that affect the velocity profile, and therefore, various coefficients should be modified to get the best LES velocity profile compared to the DNS data.
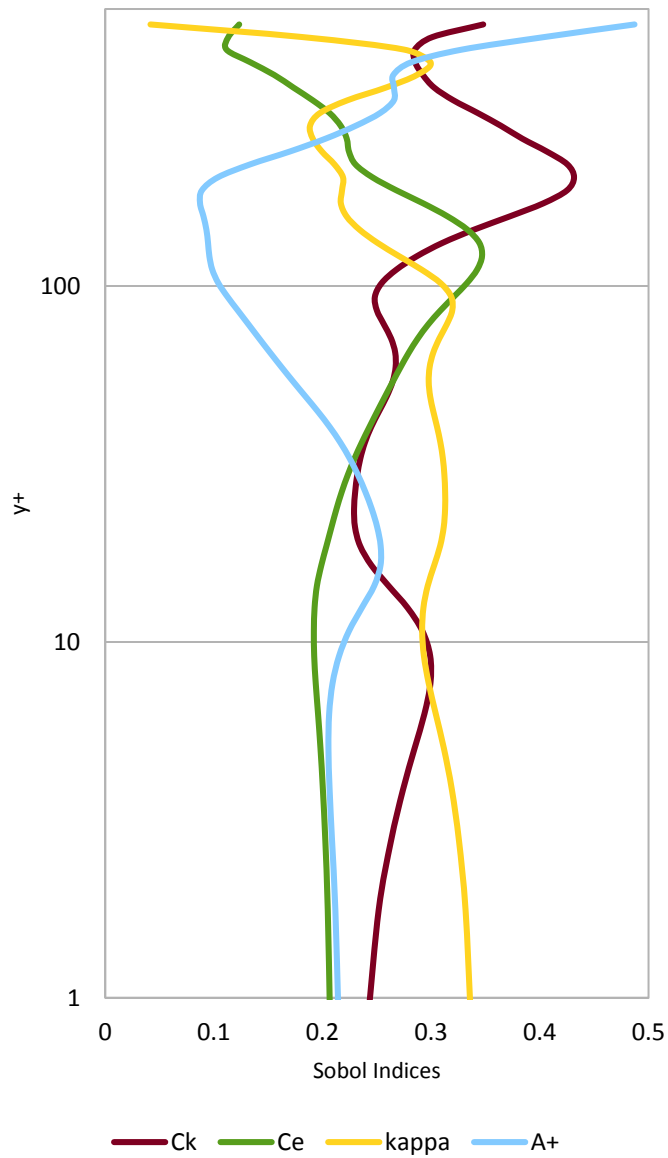
Figure 6.3 Sobol indices along the y direction for WMLES model at $Re_\tau = 550$
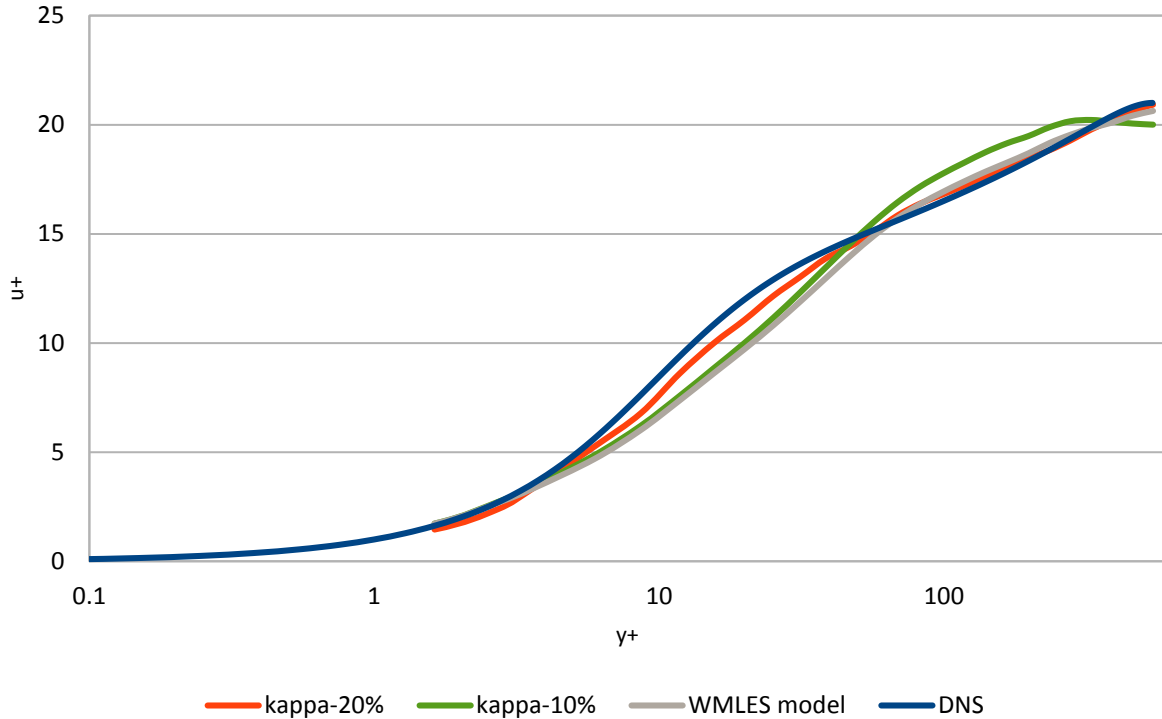
Figure 6.4 Comparison of velocity profile obtained by decreasing κ by 20% and 10% for WMLES model with DNS data at $Re_\tau = 550$

6.2   UQ of Velocity Profile when $Re_\tau = 2000$

6.2.1   UQ of Velocity Profile from Smagorinsky Model

At $Re_\tau = 2000$, it can be seen from Fig. 6.5 that the situation is similar to the when $Re_\tau = 550$ case. Along the y direction in the buffer layer ($5 < y^+ < 30$), C_k is the most significant coefficient, although C_ε become slightly more important than C_k for $200 < y^+ < 300$, however in most y^+ range Sobol index of C_k is larger. It can also be seen that after $y^+ > 30$, in log-law region, Sobol index of C_k decreases. When $y^+ > 1000$, Sobol indices of both coefficients become chaotic and irregular. It is due to the fact that when $y^+ > 1000$, the flow is in law of wake region where large scale turbulent eddies dominate.

31

Similar to the situation when Re$_\tau$ = 550, C_k is the most important coefficient. As shown in Fig. 6.6, C_k is increased by 20% (red line) and 10% (green line) and C_k with 20% increase provides a closer agreement between the simulation and DNS data.
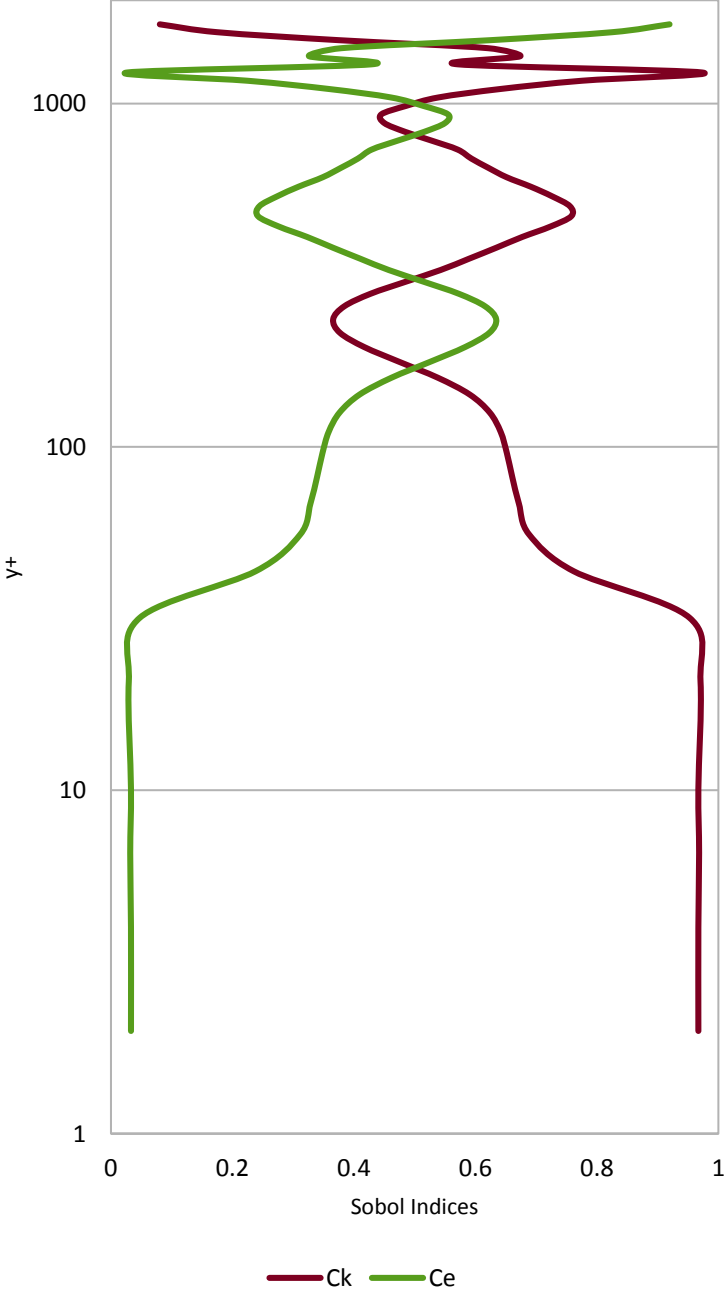
Figure 6.5 Sobol indices along the y direction for Smagorinsky model at Re$_\tau$ = 2000
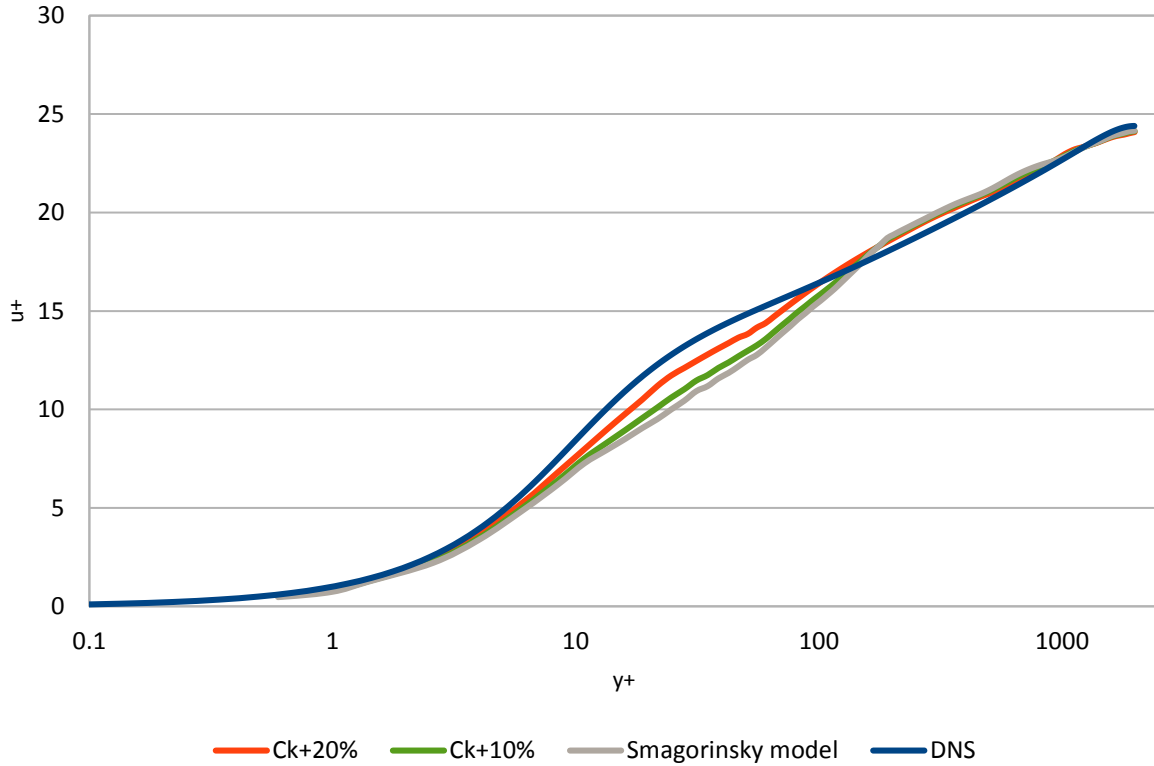
Figure 6.6 Comparison of velocity profiles obtained by increasing C_k by 20% and 10% for Smagorinsky model with DNS data at Re$_\tau$ = 2000

6.2.2 UQ of Velocity Profile for WMLES Model

For WMLES model at Re$_\tau$ = 2000, Sobol indices are shown in Fig. 6.7. This figure shows that C_k is the most influential coefficient in the viscous sublayer, but immediately decreases after that. κ and A^+ don't contribute much in this situation and keep a low value. C_ε becomes increasingly more important in the log-law region and exceed the Sobol index of C_k when y$^+$ is around 700. For y$^+$ > 1000, no significant information as the model coefficients can be obtained.

C_k is chosen as the most significant model coefficient and when it increases, velocity profile becomes closer to DNS data shown in Fig. 6.8. Red and green curves for velocity profile represent increase in C_k of 20% and 10%, respectively.

33
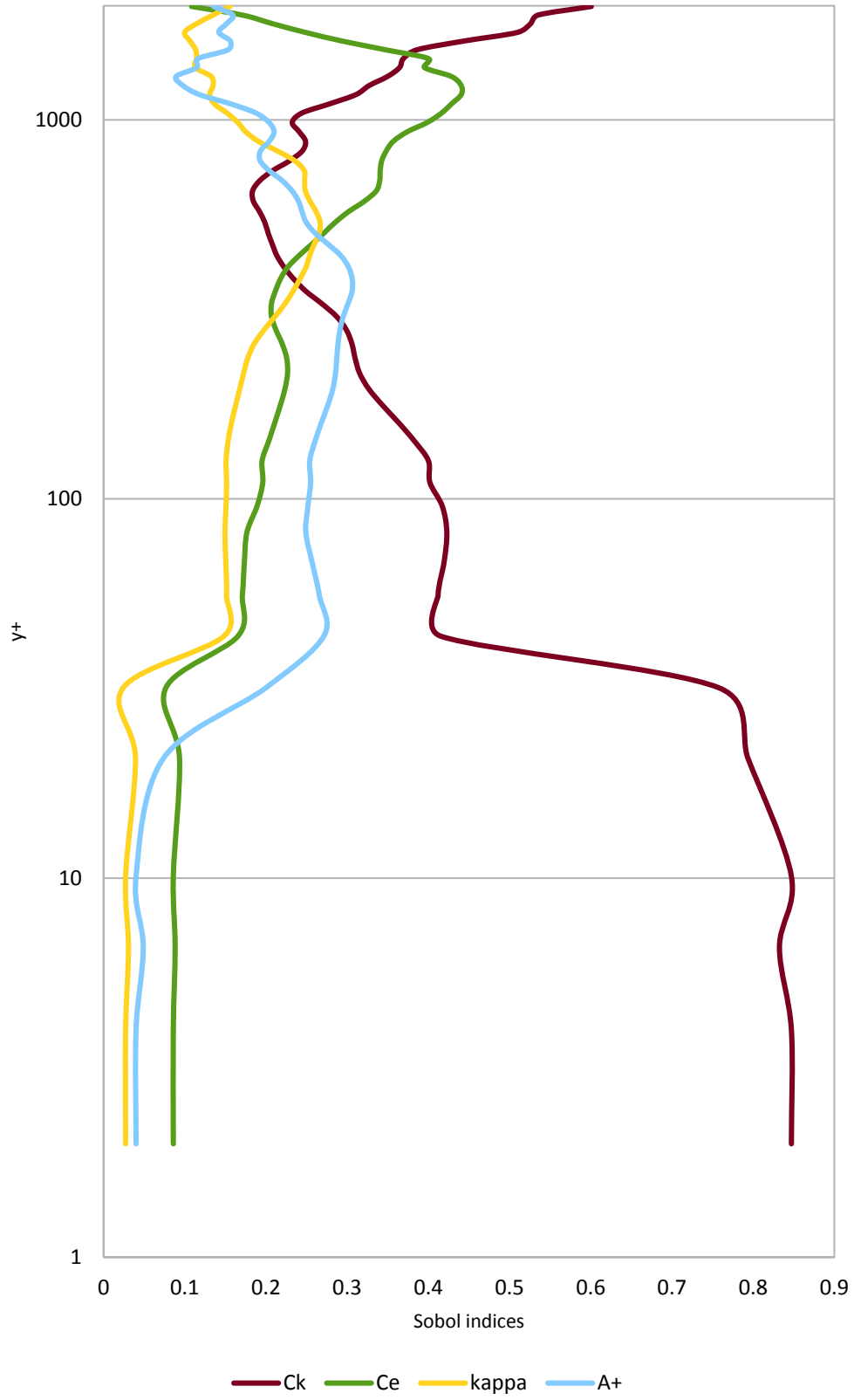
Figure 6.7 Sobol indices along the y direction for WMLES model at Re$_\tau$ = 2000
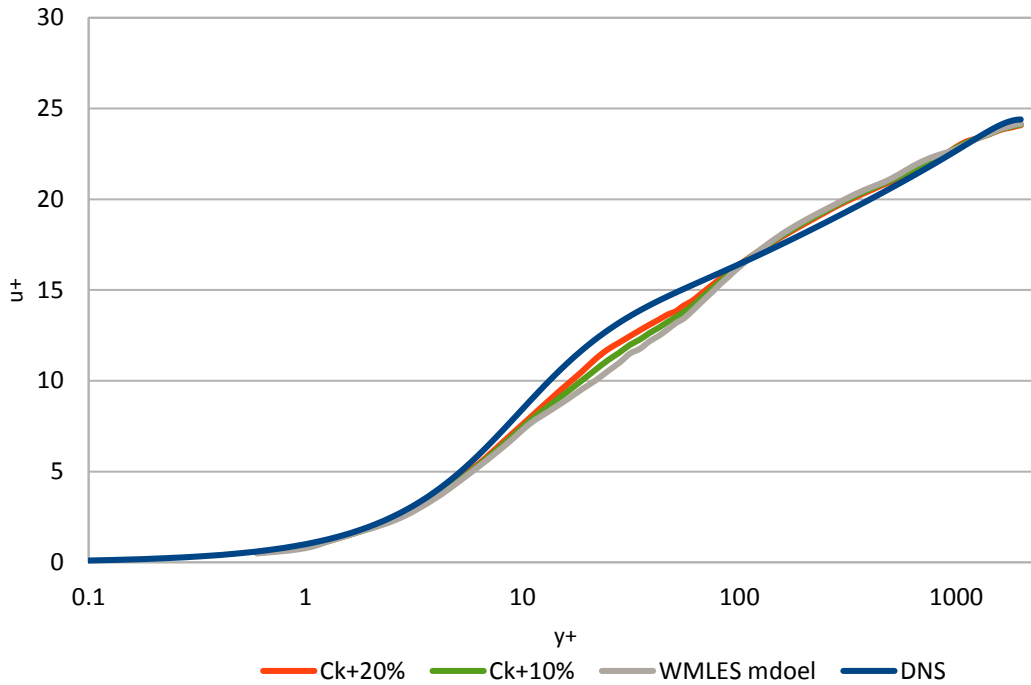
Figure 6.8 Comparison of velocity profiles obtained by increasing κ by 20% and 10% for WMLES model with DNS data at $Re_\tau = 2000$

6.3 UQ of Velocity Profile when $Re_\tau = 5200$

6.3.1 UQ of Velocity Profile from Smagorinsky Model

For $Re_\tau = 5200$, using the Smagorinsky model, the trend in Sobol indices is almost the same as in Fig. 6.5 for $Re_\tau = 2000$. Sobol indices of C_k begin to decrease in the log-law layer and remain around 0.75 until y^+ reaches 1000. However, C_k has the most influence on the mean velocity profile up to $y^+ > 1000$.

Fig. 6.10 shows the comparison of the velocity profiles with the DNS data when C_k is increased by 20% (red line) and 10% (green line); The red line with 20% increase in C_k is closer to the DNS data.
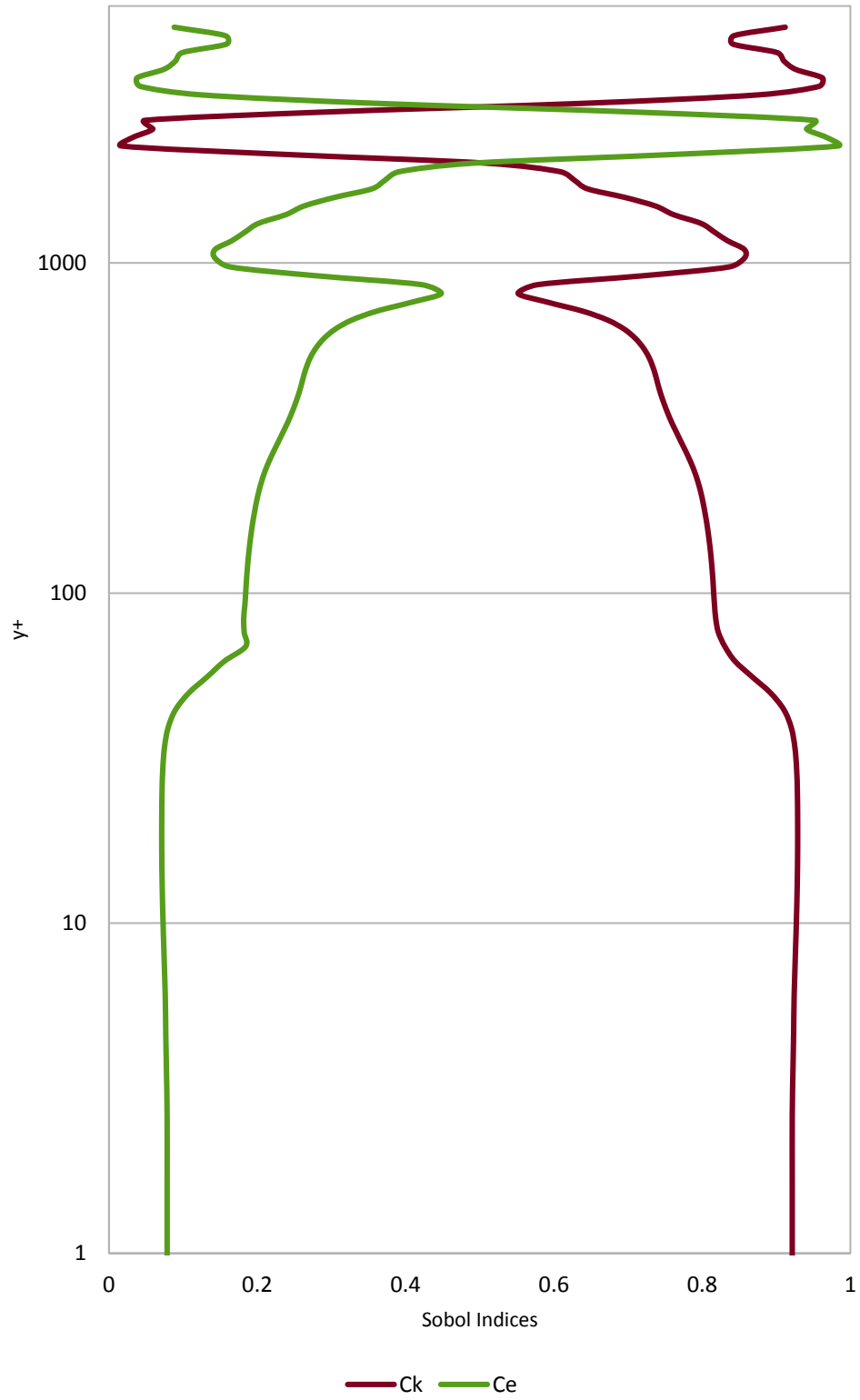
Figure 6.9 Sobol indices along the y direction for Smagorinsky model at $Re_\tau = 5200$
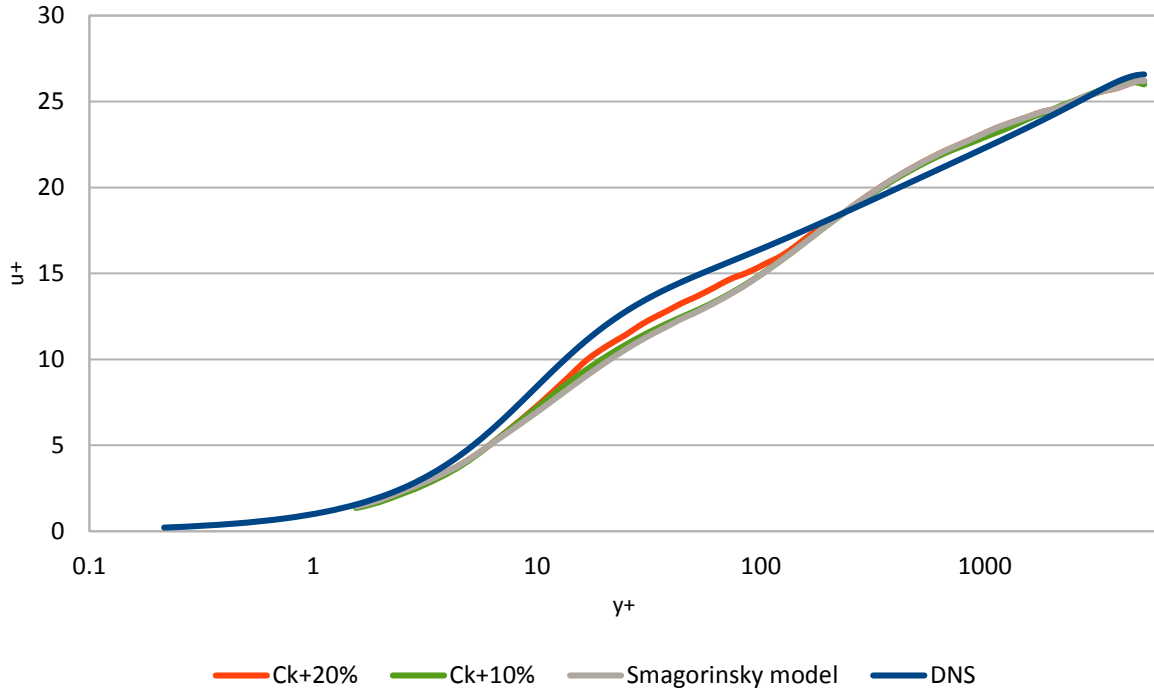
Figure 6.10 Comparison of velocity profiles obtained by increasing C_k by 20% and 10% for Smagorinsky model with DNS data at $Re_\tau = 5200$

6.3.2 UQ of Velocity Profile for WMLES Model

Fig. 6.11 shows that Sobol indices of WMLES model when $Re_\tau = 5200$. In the viscous sublayer (0 $< y^+ < 5$), κ ranks first with value of 0.93. When y^+ increases, and goes into the buffer layer, Sobol index of κ decreases and C_ε increases. Finally, C_ε dominates the influence on the mean velocity profile after the log-law region, until the outer layer. In the velocity defect layer, the Sobol indices become chaotic.

In this case, C_ε contributes most to the velocity profile. Fig. 6.12 shows the comparison of velocity profile with DNS data when C_ε decreases by 20% (red line) and 10% (green line); The red line with 20% increase in C_ε shows closer agreement with the DNS data.
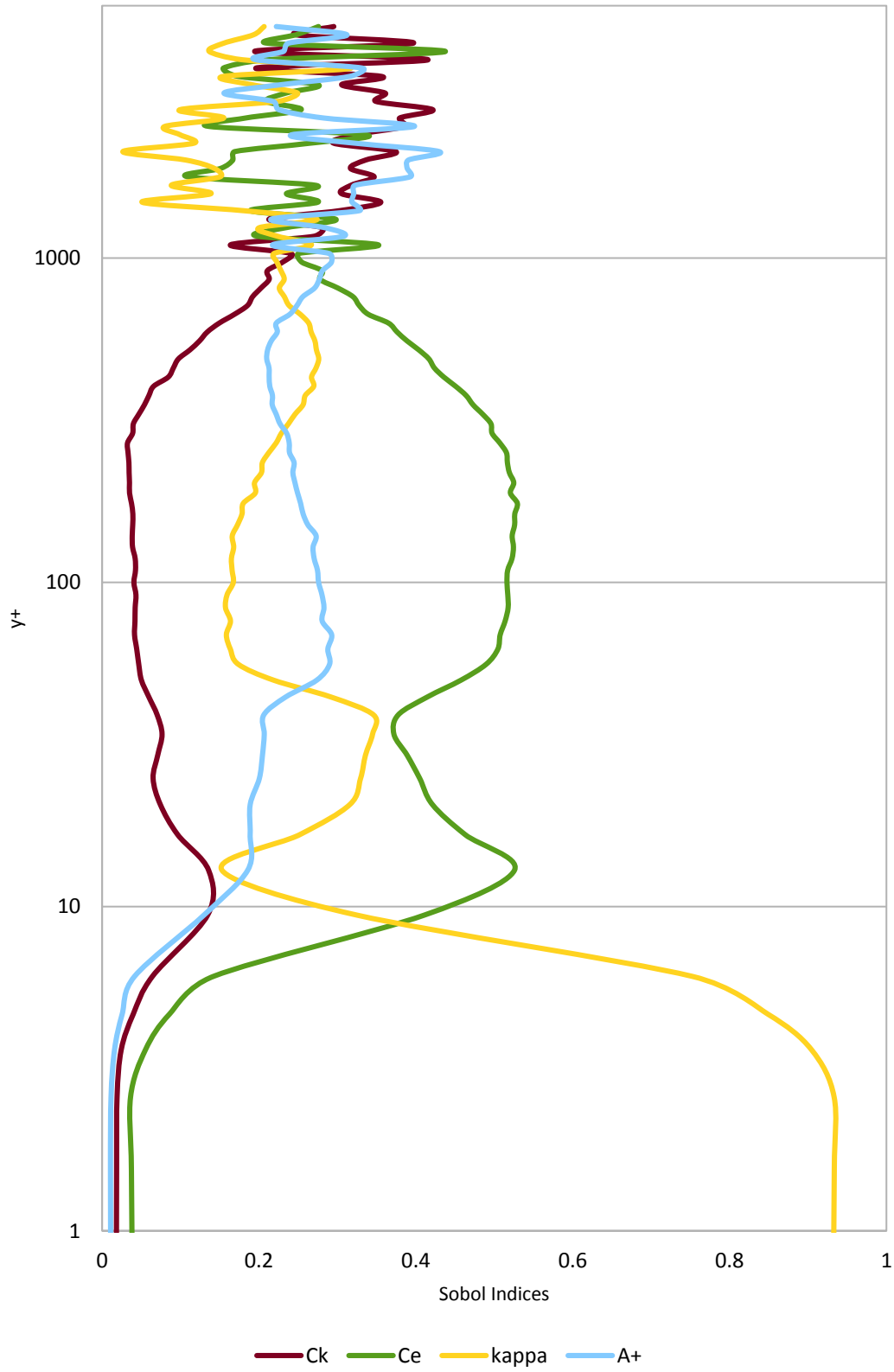
Figure 6.11 Sobol indices along the y direction for WMLES model at Re$_\tau$ = 5200
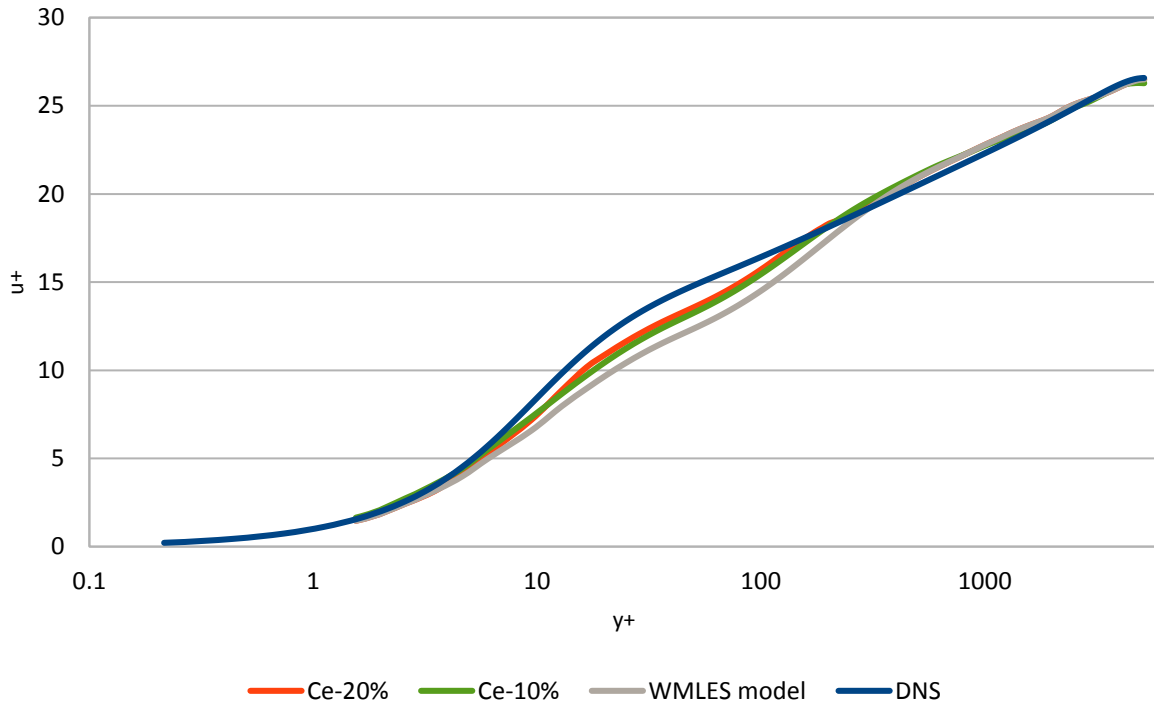
Figure 6.12 Comparison of velocity profiles obtained by decreasing C_{ε} by 20% and 10% for WMLES model with DNS data at $Re_{\tau} = 5200$

Chapter 7: Conclusions

In this thesis, an uncertainty quantification (UQ) methodology has been successfully implemented in OpenFOAM. UQ studies focusing on the closure coefficients of two LES models for tuebulent flow in a channel are performed. Two LES turbulence models considered are the Smagorinsky model and the Wall-Modeled Large Eddy Simulation (WMLES) model. Sobol Indices are used to rank the contributions of each model coefficient to total model uncertainty.

First, the LES computations of turbulent flow in the channel were validated by comparing the velocity profile obtained using the original Smagorinsky model with that obtained by the modified Smagorinsky model. Computations were then performed of Reynolds number $Re_\tau = 395, 550, 2000$ and 5200 using the Smagorinsky model and WMLES model. It was found that WMLES results were closer to the DNS data compared to Smagorinsky model results.

Uncertainty quantification due to various model coefficients was illustrated by computing the Sobol indices for skin friction coefficient and the velocity profile. In case of skin friction coefficient for the Smagorinsky model, Sobol index of model coefficient C_k increases and that of C_ε decreases with increase in Reynolds number. For WMLES model, as the Reynolds number increases, the dominant influence of C_k and C_ε is replaced by κ and A^+. For the velocity profile, in case of the Smagorinsky model, C_k was found to be the most significant coefficient at all Reynolds numbers. However for the WMLES model, κ , C_k and C_ε were the most significant coefficient for $Re_\tau = 550, 2000, 5200$ respectively. It was shown that a closer agreement in velocity profile against the DNS data could be obtained by appropriately adjusting the model coeficients.

Chapter 8: Future Work

Influence of combined variation of various model coefficients on the mean velocity profile in channel should be evaluated to further improve the LES results compared to DNS data. It will require the global UQ analysis in multi-dimensional space.

UQ analysis should also be conducted for LES computation of turbulent boundary layer on a flat plate using both the Smagorinsky and WMLES models. However, to perform the UQ analysis for this case at high Reynolds numbers requires enormous computational resources.

References

[1] J. Smagorinsky. General circulation experiments with the primitive equations I. the basic experiment. Mon. Weather Rev., 91 (3) (1963), pp. 99–164

[2] Breden D. Tracey. Machine learning for model uncertainties in turbulence models and monte carlo integral approximation. PhD dissertation, Stanford University, June 2015.

[3] David W Levy, Thomas Zickuhr, John Vassberg, Shreekant Agrawal, Richard A Wahls, Shahyer Pirzadeh, and Mchael J Hemsch. Data summary from the first AIAA computational fluid dynamics drag prediction workshop. Journal of Aircraft, 40(5):875-882, 2003.

[4] Kelly R laflin, Steven M Klausmeyer, Tom Zickuhr, John C Vassberg, Richard A Wahls, Joseph H Morrison, Olaf P Brodersen, Mark E Rakowitz, Edward N Tinoco, and Jean-Luc Godard. Data summary from second AIAA computational fluid dynamics drag prediction workshop. Journal of Aircraft, 4295):1165-1178, 2005.

[5] John C Vassberg, Edward N Tinoco, Mori Mani, David Levy, Tom Zickuhr, Dimitri J Mavriplis, Richard A Wahls, Joseph H Morrison, Olaf P Brodersen, Bernhard Eisfield, et al. Comparison of NTF experimental data with CFD predictions from the third AIAA CFD drag prediction workshop. AIAA paper, 2008-5918, 2008.

[6] John C Vassberg, Edward N Tinoco, Mori Mani, Ben Rider, Tom Zickuhr, David W Levy, Olaf P Brodersen, Bernhard Eisfield, Simone Crippa, Richard A Wahls, et al. Sumaary of the fourth AIAA CFD drag prediction workshop, AIAA paper, 2010-4547, 2010

[7] David W Levy, Kelly R laflin, Edward N Tinoco, John C Vassberg, Mori Mani, Ben Rider, Chris Rumsey, Richard A Wahls, Joseph H Morrison, Olaf P Brodersen, et al. Summary of data from the fifth AIA CFD drag prediction worshop, 2013-46, 2013.

[8] N. Wiener. The homogeneous chaos. American Journal of Mathematics，60(4):897-936, 1938.

[9] D. Xiu and G. E. Karniadakis. Modeling uncertainty in row simulations via generalized polynomial chaos. Journal of Computational Physics, 187(1):137-167, May 2003.

[10] J. B. Pleming D. S. Riha C. Waldhart L. Huyse, A. R. Bonivtch and B. H. Thacker. Verification of stochastic solutions using polynomial chaos expansions, AIAA 2006-1994. In 47th AIAA/ASME/ASCE/AHS/ASC Structures, Structural Dynamics, and Material Conference, Newport, RI, May 2006.

[11] M. S. Eldred, C. G. Webster, and P. G. Constantine. Evaluation of non-intrusive approaches for Wiener-Askey generalized polynomial chaos, AIAA 2008-1892. In 10th AIAA Non-Deterministic Approaches Forum, Schaumburg, IL, April 2008.

[12] S. Hosder and R. W. Walters. Non-intrusive polynomial chaos methods for uncertainty quantification in fluids dynamics, AIAA 2010-129. In 48th AIAA Aerospace Sciences Meeting Including the New Horizons Forum and Aerospace Exposition, Orlando, FL, January 2010.

[13] R. W. Walters and L. Huyse. Uncertainty analysis for fluid mechanics with applications. Technical report, ICASE 2002-1, NASA/CR-2002-211449, NASA Langley Research Center, Hampton, VA, 2002.

[14] H. N. Najm. Uncertainty quantification and polynomial chaos techniques in computational fluid dynamics. Annual Review of Fluid Mechanics, 41:35-52, January 2009.

[15] https://www.cfd-online.com/Forums/openfoam-solving/57889-les-turbulent-channel-flows.html

[16] http://turbulence.ices.utexas.edu/

Vita

Zuoxian Hou

Degrees	M.S. Mechanical Engineering, Washington University in St. Louis, May 2017
	B.S. Mechanical Engineering, Xi'an JiaoTong University, June 2015

May 2017